Reactivity of the β-AlF$_3$(100) surface: defects, fluorine mobility and catalysis of the CCl$_2$F$_2$ dismutation reaction†

C. L. Bailey,*[a] S. Mukhopadhyay,[b] A. Wander,[a] B. G. Searle,[a] J. M. Carr[a] and N. M. Harrison[ab]

Hybrid exchange density functional theory is used to model defects on the β-AlF$_3$ (100) surface. The stability of the surface with respect to the diffusion of surface F ions is investigated. It is shown that under typical reaction conditions (600 K) the surface is not kinetically hindered from reaching thermodynamic equilibrium. A reaction mechanism for the catalysis of 2CCl$_2$F$_2$ → CClF$_3$ + CCl$_3$F is proposed. The mechanism and corresponding reaction barriers are calculated using a double-ended transition state search method. It is predicted that the processes that determine the overall reaction rate occur at defect sites.

I. Introduction

There has been much recent interest in the use of aluminium fluoride (AlF$_3$) as a strong Lewis acid catalyst. High surface area (HS) AlF$_3$ can now be prepared with a Lewis acidity comparable to those of the widely used Swarts catalysts based on antimony pentafluoride.[1,2] Such a material is of interest as strong Lewis acid catalysts are used in the large scale production of chlorofluorocarbons (CFCs) and hydrofluorocarbons (HFCs)[3–6] for a wide range of applications including aerosol propellants, refrigerants and solvents.

The various crystalline forms of AlF$_3$ consist of arrangements of corner sharing AlF$_6$ octahedra.[7–9] The thermodynamically stable phase is α-AlF$_3$. The surfaces of α-AlF$_3$ are known to be less catalytically active than the surfaces of the β phase, which show moderate catalytic activity, and the amorphous HS materials, which show high catalytic activity.[10] Many experimental studies have been performed to investigate the structure and chemical properties of AlF$_3$, including solid state NMR,[11–13] powder X-ray diffraction,[11,12,14–18] infrared spectroscopy,[17–19] X-ray photoelectron spectroscopy[11,19,20] and temperature programmed desorption.[21] The majority of traditional surface science techniques for determining surface structure require large, pure, crystalline samples. Producing suitable AlF$_3$ crystals is very difficult. There is, consequently, very little information available on the detailed atomic-scale surface structure of these fluorides.

Ab initio modelling has recently been used to predict the structures and properties of crystalline AlF$_3$ surfaces.[22,23] It was shown that AlF$_3$ surfaces are stoichiometric as AlF$_3$ is a highly ionic material and under typical conditions the Al and F ions remain strictly Al^{3+} and F$^-$. Under-coordinated Al ions are, therefore, always exposed at the surface. The under-coordinated surface Al ions on AlF$_3$ are, similarly, predicted to display Lewis acidity and may be responsible for the catalytic nature of AlF$_3$.[23,24] It has previously been shown that under-coordinated Al ions at the surface of η-Al$_2$O$_3$ lead to its Lewis acidity.[25] A strong Lewis acid can be characterised by a large NH$_3$ binding energy and a large blue shift in the stretching frequency of adsorbed CO. The reactivities of under-coordinated Al ions on several AlF$_3$ surfaces have previously been characterised *via* the calculation of their NH$_3$ binding energies and CO stretching frequencies.[24,26] While all sites display at least moderate Lewis acidity, the sites displaying the strongest Lewis acidity consist of under-coordinated Al ions bound to five bidentate F ions.[24,26] It is predicted that such sites will not be exposed on α-AlF$_3$. They are, however, predicted to occur on the β-AlF$_3$ (100) surface which is thought to be exposed in small quantities on β-AlF$_3$ crystallites.[27]

The β-AlF$_3$ (100) surface, shown in Fig. 1, contains two inequivalent rows of ions in which alternate Al ions are under-coordinated. The uppermost row is labelled row A while the lower row is labelled row B. The surface Al ions are all coordinated to five bidentate F ions, and in addition, every alternate Al ion is also coordinated to a monodentate F ion. It is energetically favourable for monodentate F ions to cap every alternate Al ion, as in this way the structure maintains a stoichiometric surface while minimising the electrostatic repulsion between the F ions.

At finite temperatures, however, it is likely that the monodentate F ions are able to diffuse across the surface from one Al ion to another. Assuming a surface consisting of evenly distributed F ions, the movement of one F ion from above one surface Al ion to an adjacent, previously under-coordinated, Al ion will result in two F ions adjacent to one another and two under-coordinated Al ions adjacent to one another. These groupings of monodentate F ions and under-coordinated Al ions can be considered to be defect sites.

[a] Computational Science and Engineering Department, STFC Daresbury Laboratory, Daresbury, Warrington, Cheshire, WA4 4AD, United Kingdom. E-mail: christine.bailey@stfc.ac.uk; Fax: +44 (0)1925 603634; Tel: +44 (0)1925 603204
[b] Department of Chemistry, Imperial College London, Exhibition Road, London, SW7 2AZ, United Kingdom
† Electronic supplementary information (ESI) available: Tables I and II. See DOI: 10.1039/b920542j
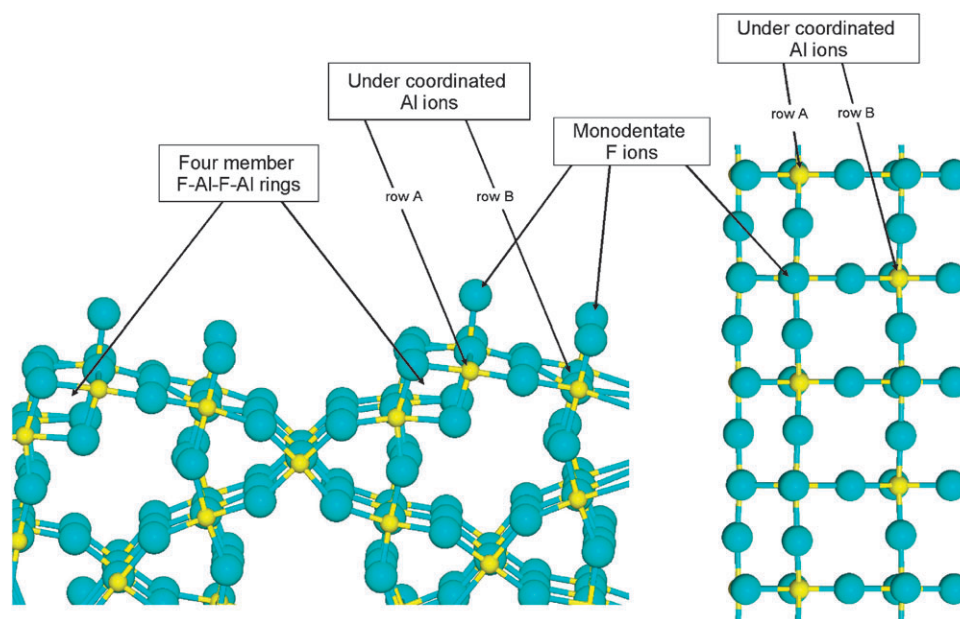
Fig. 1 A side view (left) and a plan view (right) of the β-AlF$_3$ (100) termination. The Al ions are represented by small spheres and the F ions by large spheres. The rows of surface Al ions run from top to bottom in the plan view (right).
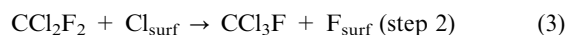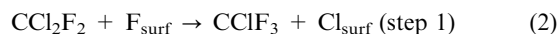
β-AlF$_3$ is known to catalyse several halide exchange reactions. One of the simplest is the dismutation of CCl$_2$F$_2$:

$$2CCl_2F_2 \rightarrow CCl_3F + CClF_3 \qquad (1)$$

Although this and similar reactions are widely used to characterise the catalytic properties of AlF$_3$ surfaces, the kinetics and mechanisms of these processes are poorly understood. The reaction given in eqn (1) proceeds on many alumina and chromia based surfaces. It is known that these surfaces do not just offer adsorption sites for the reactants, but that they are also directly involved in halogenating the reacting CCl$_2$F$_2$ molecules.[28–32] The reaction has been shown to proceed in a non-concerted manner:[32] That is, a sequence of fluorination and chlorination reactions occur at the catalyst surface.

It has previously been shown that HCl can dissociate upon adsorption at the surface of β-AlF$_3$ and that there is either no energy barrier or a very low energy barrier to the dissociation.[24] It is proposed here that CCl$_2$F$_2$ dismutation initially involves dissociation of the molecule upon adsorption. Unlike the dissociation of HCl upon adsorption though, it is expected that there is a significant energy barrier associated with the dissociation of CCl$_2$F$_2$ as, in contrast to HCl, CCl$_2$F$_2$ is not strongly polar. If the barrier is not insurmountable at elevated temperatures, then it is hypothesised that the dismutation reaction proceeds *via* a two step process, shown diagrammatically in Fig. 2. The first step involves the adsorption of a CCl$_2$F$_2$ molecule *via* its Cl atom to an under-coordinated Al ion on the surface. Subsequently, the C–Cl bond dissociates and a new C–F bond with a nearby surface F ion is formed. The newly formed CClF$_3$ molecule then desorbs, leaving a Cl ion at the surface. The second step of the dismutation reaction involves the adsorption of a second CCl$_2$F$_2$ molecule, this time *via* its F atom. The C–F bond dissociates and a bond is then formed between the C and a previously deposited Cl ion to

form a CCl$_3$F molecule, which can then desorb from the surface. This two step reaction mechanism can be written as

$$CCl_2F_2 + F_{surf} \rightarrow CClF_3 + Cl_{surf} \text{ (step 1)} \qquad (2)$$

$$CCl_2F_2 + Cl_{surf} \rightarrow CCl_3F + F_{surf} \text{ (step 2)} \qquad (3)$$

In this paper the β-AlF$_3$ surface is studied, and defect sites consisting of adjacent under-coordinated Al ions are modelled. These models are used to estimate the concentration of the defect sites at the β-AlF$_3$ (100) surface. The mobility of the monodentate F ions is studied from calculations of the transition barriers associated with their movement. The dismutation of CCl$_2$F$_2$, at the β-AlF$_3$ (100) surface is investigated. The adsorption of CCl$_2$F$_2$ to this surface is initially considered and then the structures and energetics of the transition barriers are calculated for the reactions defined in eqn (2) and (3). Reaction pathways and energetics are initially calculated on a defect free surface, and then the influence of two different modelled defect sites on step one of the reaction are
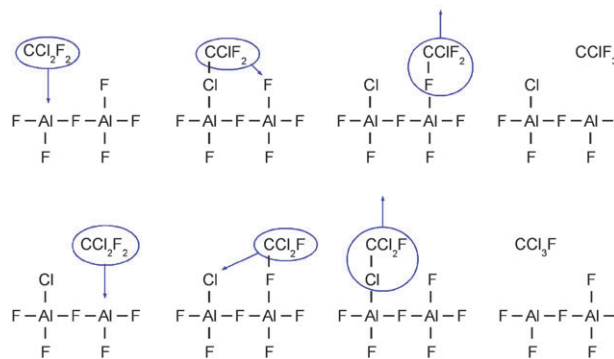
Fig. 2 The proposed reaction mechanism for the dismutation of CCl$_2$F$_2$. The upper row represents step one of the reaction and the lower row represents step two of the reaction.

considered. The energetics of the calculated pathways are analysed and transition state theory[33] is used to make an estimate of the overall turnover of the dismutation reaction at the β-AlF$_3$ (100) surface.

II. Methodology

The density functional theory (DFT) calculations were performed using CRYSTAL[34] and the B3LYP hybrid exchange functional.[35–37] This functional has been shown to provide a reliable description of geometric and electronic structure and energetics in a wide range of materials.[38,39] Polarised triple valence Gaussian basis sets were used throughout. Details of the basis sets can be found in the ESI.† In CRYSTAL, the convergence of the real space summations of the Coulomb and the exchange contributions to the Hamiltonian matrix are controlled by five overlap criteria. The control of these approximations is described in detail elsewhere.[34] The values used in this study are 10^{-8}, 10^{-8}, 10^{-8}, 10^{-8} and 10^{-16}. A shrinking factor of eight was used to define the Pack-Monkhurst net for sampling in reciprocal space and an atom centred numerical sampling grid consisting of 75 radial points and 974 angular points in the region of chemical interest (referred to in CRYSTAL as an extra large grid) was used to calculate the matrix elements of the DFT potential. This set of tolerances converges the total energy to within 10^{-4} eV per AlF$_3$ formula unit.

Locally stable structures, whose energies are of interest, were fully optimised using a conjugate gradient algorithm. The structures were considered to be converged when the residual absolute forces along all allowed symmetry directions were below 1.0×10^{-2} eV Å^{-1}. Transition state structures were identified using the nudged elastic band (NEB) algorithm.[40,41] This algorithm has only recently been implemented in CRYSTAL[42] and the current work represents the first instance of the implementation being used to calculate reaction pathways and barriers for surface catalysed reactions. Transition structures were considered converged when the residual absolute forces along all allowed symmetry directions were below 2.6×10^{-2} eV Å^{-1}. The computational cost of converging to a transition state using the NEB algorithm is very high; consequently, the tolerances used in our CRYSTAL calculations and the thicknesses of our slabs were reduced for these calculations. The values of the five overlap criteria were reduced to 10^{-6}, 10^{-6}, 10^{-6}, 10^{-6} and 10^{-12}, a shrinking factor of two was used to define the Pack-Monkhurst net and an atom centred numerical grid consisting of 75 radial points and 434 angular points (referred to in CRYSTAL as a large grid) was used. The slab thicknesses (defined as the vertical distance between the Al ions on row A of the slab) were reduced from 13.8 Å (26 Al ions per (1 × 1) slab) to a distance of 10.2 Å (20 Al ions per (1 × 1) slab). The effects of these approximations are well controlled and are discussed in section III.B.

The structure of the low energy β-AlF$_3$ (100) (1 × 1) termination was obtained from a previous computational study[22] and is shown in Fig. 1. The surface contains four Al sites, (two on row A and two on row B) and two monodentate F ions (one on each row) per (1 × 1) unit cell. This (1 × 1) cell can be represented by $\left[\begin{smallmatrix} \circ & \bullet \\ \bullet & \circ \end{smallmatrix}\right]$, where the two rows of circles

represent rows A and B. The filled circles represent surface F ions above Al ions while the unfilled circles represent under-coordinated Al ions. To obtain accurate energies for the formation of particular defects, calculations must be performed within cells large enough to contain a given defect and a buffer zone in which the F ions are arranged in their thermodynamic equilibrium positions. This removes the effects of defect-defect interactions.

Defects consisting of two adjacent F ions along row A can be calculated within a (5 × 1) cell. This cell contains two such defects and can be represented by $\left[\begin{smallmatrix} \circ & \bullet & \bullet & \circ & \bullet & \circ & \bullet & \bullet & \circ \\ \bullet & \circ & \circ & \bullet & \circ & \bullet & \circ & \circ & \bullet \end{smallmatrix}\right]$. It is not possible to model a single defect of this type without introducing a second defect due to the periodicity of the system. A similar calculation was performed to calculate the energy associated with two adjacent F ions along row B. To predict the number of double defects, that is the formation of three adjacent F ions on one row and three adjacent under-coordinated Al ions on the other row, surface energies within a (3 × 1) cell, $\left[\begin{smallmatrix} \bullet & \circ & \circ & \circ & \bullet & \circ \\ \circ & \bullet & \bullet & \bullet & \circ & \bullet \end{smallmatrix}\right]$, were calculated.

The ratio of the number of defect sites (consisting of two or three adjacent F ions) to the total number of monodentate F ions at thermodynamic equilibrium is

$$\frac{n}{N} = \sum_i \exp\left(\frac{-\Delta E_i}{kT}\right), \qquad (4)$$

where n and N are the total number of defect sites and monodentate F ions respectively, k is the Boltzmann constant, T is the absolute temperature and ΔE_i is the energy difference between the ground state surface and the surface containing a defect of type i. In order to predict the number of defects to an accuracy of 50% at 600 K, the defect energy must be calculated to within an accuracy of 0.02 eV per defect.

The transition state structures and energy barriers for the diffusion of F ions between neighbouring Al ions were calculated using the NEB algorithm. The F ions can either move along the rows in the crystallographic $\langle 001 \rangle$ direction or perpendicular to the rows in the $\langle 010 \rangle$ direction. Two different mechanisms for the diffusion of F ions were considered. The first mechanism, denoted here as 'direct', involves an F ion moving directly from one Al ion to another. The second mechanism, labelled 'indirect', involves the concerted motion of two F ions: A monodentate F ion displaces an F ion that is bound between the two adjacent Al ions and then the displaced F ion becomes a monodentate F ion above the second Al ion. The direct mechanism is shown on the left hand side of Fig. 3 and 4 and the indirect mechanism is shown on the right hand side of these two figures.

Binding energies were calculated for the adsorption of CCl$_2$F$_2$ to under-coordinated Al ions on the β-AlF$_3$ (100) (1 × 1) surface. Adsorption *via* both a Cl and an F were considered. In addition, adsorption at several different orientations about the molecule's axis perpendicular to the surface was considered. Calculations were also performed within (2 × 1) cells to enable an estimate of the binding energies at low coverages. The calculated binding energies (a negative value denotes binding between the surface and molecule) were corrected for basis set superposition error (BSSE) using the counterpoise scheme.[43] As the absolute

6126 | *Phys. Chem. Chem. Phys.*, 2010, **12**, 6124–6134

This journal is © the Owner Societies 2010
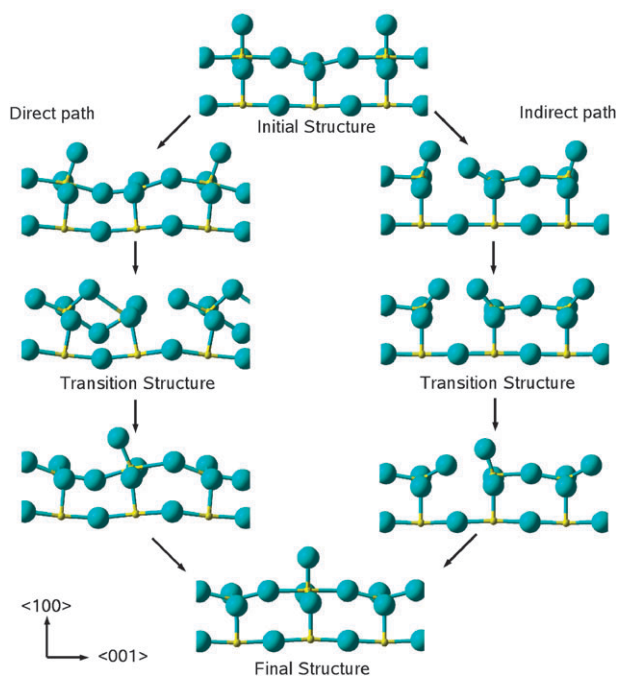
Fig. 3 Reaction pathways for the diffusion of an F ion along row A (in the $\langle 001 \rangle$ direction). The left hand side shows the direct pathway and the right hand side shows the indirect pathway. The structures shown between the end points and transition states represent geometries along the minimum energy pathway. The Al ions are represented by small spheres and the F ions by large spheres.
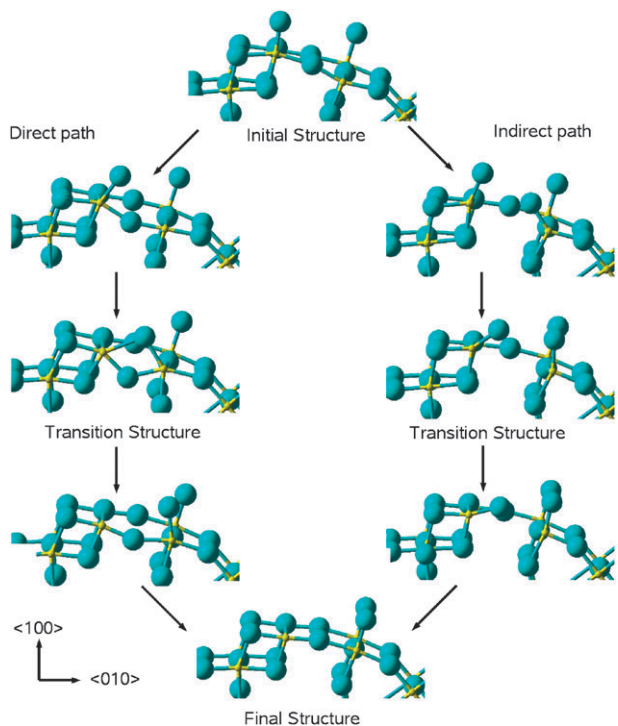
Fig. 4 Reaction pathways for the diffusion of an F ion from row A to row B (in the $\langle 010 \rangle$ direction). The left hand side shows the direct pathway and the right hand side shows the indirect pathway. The structures shown between the end points and transition states represent geometries along the minimum energy pathway. The Al ions are represented by small spheres and the F ions by large spheres.

binding energies are relatively small, the corrections for BSSE are significant. The binding energies are quoted before and after BSSE correction and the accuracy of these calculations is discussed in section III.C. Transition state structures and energy barriers were calculated using the NEB algorithm for several different end point configurations for the reactions described by eqn (2) and (3). BSSE corrections have not been applied to the transition state energy barriers because, to a reasonable approximation, the BSSE correction of the initial state and the BSSE correction of the transition state will cancel one another.

III. Results and discussion

A. Stable structures

The calculated defect energies are given in Table 1 along with the predicted ratio of the number of defects to the total number of surface F ions at 300 K and 600 K. The predominant defect consists of two adjacent F ions on row A and two adjacent under-coordinated Al ions on row B $\left[\begin{smallmatrix} \circ & \bullet & \bullet & \circ \\ \bullet & \circ & \circ & \bullet \end{smallmatrix}\right]$. (Note: This diagram represents the local environment of the defect, rather than the (5×1) cell that was used to calculate the energy of the defect.) The preference for adjacent F ions on row A as opposed to row B may be due to the distorted environment around the Al ions along row A; two of the F ions that neighbour these Al ions are part of a constrained Al-F-Al-F ring (see Fig. 1). In our previous study[44] of NH_3 adsorption to this surface, we showed that NH_3 binds to Al ions on row A with a binding energy of around -2.0 eV compared to -1.9 eV for Al ions on row B. Analysis of the results presented here suggests that, similarly, the Al ions on row A also bind monodentate F ions more strongly than the Al ions on row B.

B. Fluorine mobility

As the calculation of reaction barriers is computationally expensive, the effect of using thinner slabs and lower numerical tolerances (as discussed in section II) on the computed reaction barriers was considered. The transition energy barriers for the direct diffusion of F ions from row A to row B, using different approximations, are shown in Table 2. The transition energy barrier is consistent to within 0.05 eV in all approximations. Transition state energies have, therefore, been calculated using thin slabs and lower numerical accuracy in all subsequent NEB calculations.

Approximate minimum energy pathways were calculated for the direct and indirect movement of F ions along the $\langle 010 \rangle$ and $\langle 001 \rangle$ directions within a (1×1) cell. The transition state energies, relative to the defect free surface, are given in Tables 3 and 4 for the direct and indirect pathways, respectively. Selected bond lengths for the transition state structures are also given in these tables. It can be seen that in half of the cases considered it is energetically favourable for the F ions to move directly from one site to another, while in the remaining cases it is favourable for the diffusion to occur indirectly *via* an intermediate F ion. Structures along the direct and indirect reaction pathways for the movement of F ions along row A are shown in Fig. 3, and structures for the movement of F ions from row A to row B are shown in Fig. 4.

This journal is © the Owner Societies 2010

Phys. Chem. Chem. Phys., 2010, **12**, 6124–6134 | 6127

Table 1 The defect energies, relative to the defect free surface, associated with two or three adjacent F ions on either row A or row B. The ratios of the number of defect sites to the total number of surface F ions at 300 K and 600 K (calculated using eqn (4)) are also shown. The diagrams in the first column of the table represent the local environment of the defects, rather than the cells that were used to calculate the defect energies

		Ratio of (no. of defects) : (no. of surface F ions)	
Description of defect	Defect energy ΔE_i (eV)	300 K	600 K
2 adjacent F ions on row A $\left[\begin{smallmatrix}\circ\bullet\bullet\circ\\\bullet\circ\circ\bullet\end{smallmatrix}\right]$	0.13	1 : 150	1 : 12
2 adjacent F ions on row B $\left[\begin{smallmatrix}\bullet\circ\circ\bullet\\\circ\bullet\bullet\circ\end{smallmatrix}\right]$	0.38	1 : 2 400 000	1 : 1600
3 adjacent F ions on row A $\left[\begin{smallmatrix}\circ\bullet\bullet\bullet\circ\\\bullet\circ\circ\circ\bullet\end{smallmatrix}\right]$	0.38	1 : 2 400 000	1 : 1600
3 adjacent F ions on row B $\left[\begin{smallmatrix}\bullet\circ\circ\circ\bullet\\\circ\bullet\bullet\bullet\circ\end{smallmatrix}\right]$	0.88	1 : 6.2×10^{14}	1 : 25 000 000

Table 2 Transition state and final state energies, relative to the initial structure, calculated using different slab thicknesses and different levels of numerical accuracy for the direct movement of an F ion from row A to row B on the β-AlF$_3$ (100) surface

No. of Al ions in slab	Numerical accuracy	Relative transition energy (eV)	Relative final energy, ΔE (eV)
26	High	2.11	1.03
26	Low	2.07	1.03
20	Low	2.15	0.84

Table 3 The transition state structures and energetics for the direct pathway. The bridging F ions are labelled F$_{bri}$ and the F ions that are moving between Al ions are labelled F$_{dif}$. The subscript on the Al denotes the coordination of the Al ion. The subscript on the F in the first column of the table denotes the row that the F ion is initially on

			Rate constant (s^{-1})		Bond lengths (Å)				
F ion	Direction of diffusion	Energy barrier, $\Delta E^{\ddagger}$ (eV)	300 K	600 K	Al$_6$–Al$_5$	Al$_6$–F$_{dif}$	Al$_6$–F$_{bri}$	Al$_5$–F$_{dif}$	Al$_5$–F$_{bri}$
F$_A$	$\langle 010 \rangle$	2.15	5 × 10^{-24}	8 × 10^{-6}	3.14	2.22	1.75	1.89	1.85
F$_B$	$\langle 010 \rangle$	1.11	2 × 10^{-6}	5 × 10^3	2.97	1.81	1.90	1.92	1.83
F$_A$	$\langle 001 \rangle$	1.33	5 × 10^{-10}	7 × 10^1	3.24	1.76	2.03	2.43	1.73
F$_B$	$\langle 001 \rangle$	1.22	3 × 10^{-8}	6 × 10^2	3.13	1.99	1.89	2.02	1.77

Table 4 The transition state structures and energetics for the indirect pathway. The subscript on the Al denotes the coordination of the Al ion. The subscript on the F in the first column of the table denotes the row that the F ion is initially on

			Rate constant (s^{-1})		Bond lengths (Å)			
F ion	Direction of diffusion	Energy barrier, $\Delta E^{\ddagger}$ (eV)	300 K	600 K	Al$_6$–Al$_5$	F–F	Al$_6$–F	Al$_5$–F
F$_A$	$\langle 010 \rangle$	1.39	4 × 10^{-11}	2 × 10^1	4.23	2.86	1.64	1.64
F$_B$	$\langle 010 \rangle$	1.33	5 × 10^{-10}	7 × 10^1	4.21	2.83	1.64	1.64
F$_A$	$\langle 001 \rangle$	1.00	2 × 10^{-4}	4 × 10^4	3.81	2.53	1.62	1.62
F$_B$	$\langle 001 \rangle$	1.35	2 × 10^{-10}	5 × 10^1	3.81	2.58	1.63	1.63

The transition state structures for the direct pathways (left hand side of Fig. 3 and 4) consist of distorted four member (-Al-F-Al-F-) rings. The energy barriers vary considerably for diffusion along the $\langle 010 \rangle$ direction, depending on whether the F ions are moving from row A to row B or from row B to row A. This asymmetry is related to the different geometry of the two sites. The vertical distance between the fully-coordinated Al ion in row A and the under-coordinated Al ion in row B is 1.6 Å compared with 0.8 Å between the fully-coordinated Al ion in row B and the under-coordinated Al in row A; consequently, it is easier for an F ion to move from row B to row A than to move from row A to row B.

The transition state structures for the indirect pathways (right hand side of Fig. 3 and 4) consist of two under-coordinated Al ions each bound to four bidentate F ions and a monodentate F ion. The bond lengths between the Al and monodentate F ions are around 1.6 Å, which is typical for monodentate F ion bonding. The transition state structures

and energetics are generally very similar for each of the different indirect reaction pathways. The exception is that the transition state energy for movement along row A is significantly lower (1.0 eV). Analysis of this transition state structure suggests that it differs from other transition state structures only in that the F ions directly below the under-coordinated Al ions are displaced along the $\langle 001 \rangle$ direction, distorting the truncated octahedra around the Al ions and reducing the total energy of the system.

The rate constants, k_i, for the diffusion of F ions were estimated using harmonic transition state theory,

$$k_i = f \frac{kT}{h} \exp\left(\frac{-\Delta E_i^{\ddagger}}{kT}\right) \qquad (5)$$

where $\Delta E_i^{\ddagger}$ is the transition state energy barrier. f is the ratio of the vibrational partition functions of the transition and initial states, where the quantity for the transition state does not

include the reactive mode. This value is approximated to unity, as to a first approximation, the partition functions of the initial and transition states are of the same order of magnitude, hence the ratio of the two is close to one. The reaction rates vary linearly with this factor, compared with exponentially with the energy barrier, hence, this is an appropriate approximation. The resulting rate constants at 300 K and 600 K for each of the pathways are given in Tables 3 and 4. At 300 K the surface F ions are predicted to be effectively immobile. At 600 K, however, the F ions are predicted to move rapidly: On a scale of several hops every ms for F ions diffusing from row A to row B. It is, therefore, predicted that at 600 K the kinetic barriers associated with the diffusion processes will not hinder the surface from achieving its thermodynamically stable phase.

C. Molecular adsorption of CCl_2F_2

Various geometries for the adsorption of CCl_2F_2 on the (defect free) β-AlF$_3$ (100) surface were considered. These include adsorption *via* the molecule's F or Cl atoms to Al ions on either row A or row B of the surface. The CCl_2F_2 molecules were adsorbed in a number of different orientations about the Al–(Cl,F)–C axis and the largest binding energies, as a function of orientation, are shown in Table 5. Structures consisting of CCl_2F_2 adsorbed F down and Cl down on row A are shown in Fig. 5. In the case of adsorption *via* the Cl atom a second adsorption geometry, in which the molecule is rotated by approximately 180° about the axis perpendicular to the surface, is also shown (Fig. 5c). This geometry is used in section III.D as the starting point for the NEB pathway that involves the formation of CClF$_3$ on row B as the C atom is significantly closer to the F ion on row B compared to the structure shown in Fig. 5b.

The adsorption energies are relatively small: For comparison NH$_3$ binds with a binding energy of up to −2.0 eV. We have previously shown that the binding energy of molecules to the surface is dominated by electrostatic interactions.[44] Analysis of the Mulliken population of isolated molecules shows that the halide atoms of CCl_2F_2 are much less negatively charged than the N atom in NH$_3$, this may explain why CCl_2F_2 only binds weakly to the surface. In addition, there is electrostatic repulsion between the neighbouring surface F ions and the CCl_2F_2 molecules and also inter-molecular repulsion between neighbouring CCl_2F_2 molecules, both of which reduce the magnitude of the binding energy.

To estimate the effect of the repulsion between CCl_2F_2 molecules and F ions, the adsorption of CCl_2F_2 on row A when all of the monodentate F ions were on row B was calculated as the distances between the CCl_2F_2 and monodentate F ions are increased in this geometry. The molecule was found to bind significantly more strongly than when the monodentate F ions were distributed between both rows. The resulting binding energy was around 0.2 eV stronger (−0.38 eV or −0.25 eV after correction for BSSE). To estimate the repulsion between neighbouring CCl_2F_2 molecules, calculations were performed at a quarter monolayer coverage in a (2 × 1) cell. It was found that CCl_2F_2 binds more strongly, by around 0.04 eV, when the coverage was decreased from a half monolayer to a quarter monolayer (the minimum distance between neighbouring CCl_2F_2 molecules is increased from 5.3 Å to 9.3 Å).
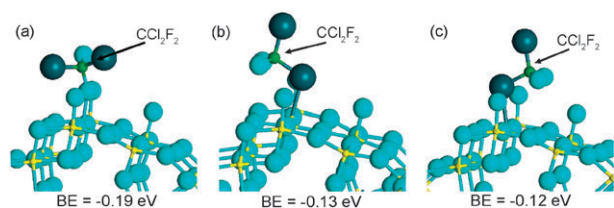
The correction for BSSE to the binding energies is approximately 0.1 eV, although this is a typical correction for BSSE, it is a large proportion of the total calculated binding energies. This implies that the geometries are unlikely to be fully optimised to their BSSE corrected minimum energy structures. Furthermore, as the counterpoise scheme yields an upper bound on the magnitude of the BSSE, the BSSE corrected energies are likely to be less negative than the true binding energies. It is, therefore, reasonable to assume that the binding energies lie between the BSSE corrected and uncorrected values presented.

To obtain estimates of the binding energies of CCl_2F_2 to under-coordinated Al ions on the (defect free) β-AlF$_3$ (100) surface at low coverages, the following approximations have been made in the light of the preceding discussions. The average binding energy, at half monolayer coverage, before and after corrections for BSSE has been used. The overall binding energy is extrapolated to the dilute limit by reducing its magnitude by 0.05 eV to account for intermolecular repulsion. The repulsion between a CCl_2F_2 molecule and an adjacent monodentate F ion is estimated to be 0.1 eV. At defect sites, when the molecule is adsorbed to an under-coordinated Al ion that has either one or no neighbouring F ions (as opposed to two on the defect free surface), the binding energy is, therefore, increased in magnitude by 0.1 eV per missing F ion. Applying these approximations, the computed binding energy is −0.15 eV, −0.25 eV and −0.35 eV for a CCl_2F_2 adsorbed *via* its Cl atom when it is neighbouring two, one and zero F ions respectively. Similarly, the binding energy is −0.20, −0.30 or −0.40 eV when the molecule is bound *via* its F atom, depending on the number of neighbouring F ions. Given the approximations made here, the resultant binding energies have been quoted to the nearest 0.05 eV.

D. Reaction mechanisms and barriers

Minimum energy paths and transition state energy barriers were calculated for movement of the CFC molecule along row A, along row B and between the rows on the defect free β-AlF$_3$ (100) surface for both steps of the reaction (defined by eqn (2) and (3)). The results from these calculations are summarised in Tables 6 and 7. The lowest transition state barriers for each step of the reaction occur when the molecule moves between rows.

The lowest energy pathways found for the first and second steps of the reaction are shown in Fig. 6 and 7, respectively.

Fig. 5 Adsorption of CCl_2F_2 on row A of the β-AlF$_3$(100) surface, (a) adsorption *via* an F atom, (b) and (c) adsorption *via* a Cl atom. The displayed binding energies have not been corrected for BSSE.

This journal is © the Owner Societies 2010

Phys. Chem. Chem. Phys., 2010, **12**, 6124–6134 | 6129

Table 5 The binding energies (with and without corrections for BSSE) for CCl_2F_2 adsorbed at half monolayer coverage on the β-AlF$_3$ (100) (1 × 1) surface

Adsorption ion	Site of adsorption	Binding energy (eV)	
		No BSSE correction	With BSSE correction
F	row A	−0.19	−0.08
F	row B	−0.18	−0.08
Cl	row A	−0.13	−0.03
Cl	row B	−0.14	−0.03

Table 6 The computed energetics and geometries of the transition states for the reaction $CCl_2F_2 + F_{surf} \rightarrow CClF_3 + Cl_{surf}$ on the defect free β-AlF$_3$ (100) surface

CCl$_2$F$_2$ adsorption site	CClF$_3$ adsorption site	Energy barrier, $\Delta E^{\ddagger}$ (eV)	Al–Cl (Å)	Al–F (Å)	C–Cl (Å)	C–F (Å)	∠F–C–Cl (degrees)
Row A	Row A	1.67	2.29	1.72	2.82	2.32	118
Row B	Row B	1.72	2.28	1.71	3.00	2.50	101
Row A	Row B	1.67	2.25	1.71	3.12	2.82	81
Row B	Row A	1.48	2.25	1.69	3.26	3.24	76

Table 7 The computed energetics and geometries of the transition states for the reaction $CCl_2F_2 + Cl_{surf} \rightarrow CCl_3F + F_{surf}$ on the defect free β-AlF$_3$ (100) surface

CCl$_2$F$_2$ adsorption site	CCl$_3$F adsorption site	Energy barrier, $\Delta E^{\ddagger}$ (eV)	Al–Cl (Å)	Al–F (Å)	C–Cl (Å)	C–F (Å)	∠F–C–Cl (degrees)
Row A	Row A	1.09	2.27	1.71	3.21	2.72	72
Row B	Row B	1.10	2.28	1.70	3.13	2.82	70
Row A	Row B	0.89	2.24	1.71	3.61	2.84	74
Row B	Row A	0.99	2.22	1.71	3.61	2.87	78

The first step involves the adsorption of a CCl_2F_2 molecule to row A (Fig. 5c) followed by the cleavage of the C–Cl bond and the formation of a $CClF_3$ molecule adsorbed on row B. The transition state barrier associated with this mechanism is 1.48 eV. The pathway for the second step involves the adsorption of a CCl_2F_2 molecule to an Al on row A of a partially chlorinated surface and the subsequent formation of a CCl_3F molecule on row B. The transition state barrier associated with this mechanism is appreciably lower, at 0.89 eV. There are many similarities between the transition state structures of both of these reactions, although the distribution of the surface F and Cl ions differs between the two structures: The surface F ions are distributed amongst the rows for the first step of the reaction but are all on row A for the second step. This suggests that the energy barriers may depend on the initial positions of the surface F and Cl ions.

The reaction pathways for the formation of a $CClF_3$ molecule on row A (step 1) were calculated after adsorption of a CCl_2F_2 molecule at defect sites that consisted of either two or three adjacent under-coordinated Al ions on row B ($\begin{bmatrix}\circ\bullet\bullet\circ\\\circ\circ\circ\bullet\end{bmatrix}$ and $\begin{bmatrix}\circ\bullet\bullet\bullet\circ\\\bullet\circ\circ\circ\bullet\end{bmatrix}$). In section III.A the structures and energies of these defects where calculated within (3 × 1) and (5 × 1) cells, respectively. It is, currently, prohibitively expensive to run NEB calculations on such large cells. The defect consisting of two adjacent Al ions was, therefore, modelled within a (2 × 1) cell $\begin{bmatrix}\bullet\bullet\circ\bullet\\\circ\circ\bullet\circ\end{bmatrix}$. In this cell, the CCl_2F_2 is adsorbed to an Al ion that neighbours one under-coordinated Al ion and one fully-coordinated Al ion. The transition state energy barrier for this reaction was calculated to be 1.22 eV. The defect consisting of three adjacent under-coordinated Al ions was modelled within a (1 × 1) cell where all the F ions were adsorbed to row A.

The transition state energy barrier for this reaction was calculated to be 1.04 eV. In the following section the energy barriers, the number of defect sites and the binding energies of the adsorbed molecules are used to predict the kinetics of the overall reaction.

E. Analysing the reaction kinetics

The small binding energies associated with adsorption of CCl_2F_2 imply that the overall coverage of the surface will be very low under typical reaction conditions (i.e. at temperatures of around 600 K). In equilibrium the chemical potential of a gas phase CCl_2F_2 molecule and an adsorbed CCl_2F_2 molecule must be equal to one another:[45]

$$\mu_{gas} = \mu_{ads}. \qquad (6)$$
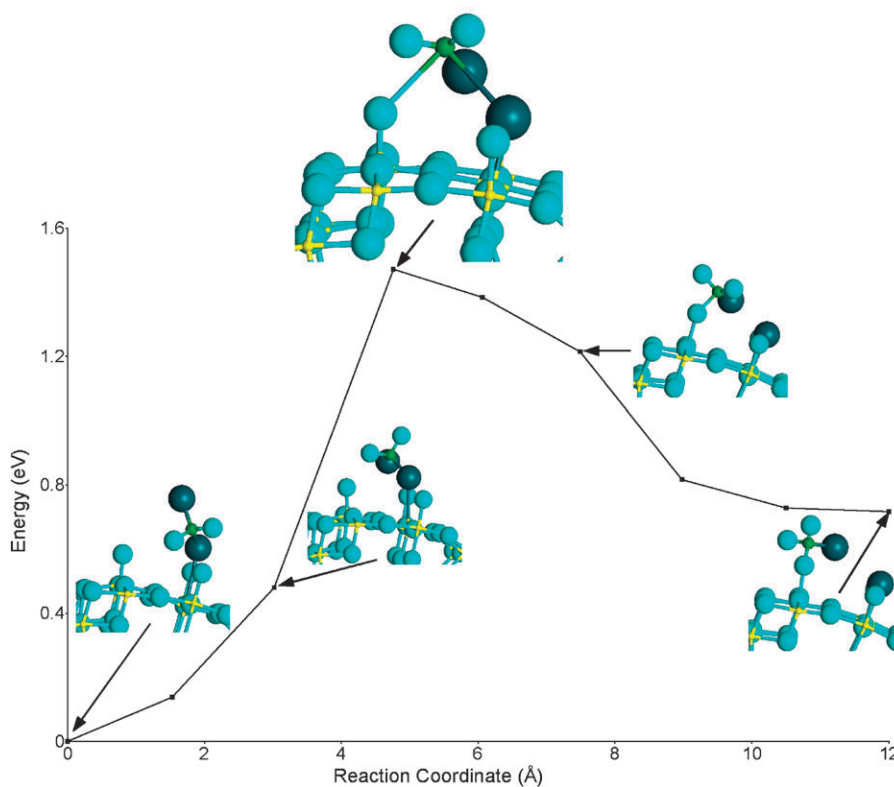
The chemical potential of an adsorbed molecule is given by

$$\mu_{ads} = kT \ln\left[\frac{\theta}{1-\theta} \cdot \frac{1}{q}\right], \qquad (7)$$

where θ is the fraction of the surface sites that are covered by an adsorbed molecule. The single particle partition function, q, is given by

$$q = \exp\left(\frac{-E_{ads}}{kT}\right) \cdot q_{vib}, \qquad (8)$$

where q_{vib} is the vibrational partition function of the adsorbed molecule. The chemical potential of an ideal gas is given by

$$\mu_{ideal\,gas} = -kT \ln\left[\left(\frac{2\pi m_i kT}{h^2}\right)^{\frac{3}{2}} \frac{kT}{p_i}\right], \qquad (9)$$

6130 | *Phys. Chem. Chem. Phys.*, 2010, **12**, 6124–6134

This journal is © the Owner Societies 2010

Fig. 6 The lowest energy pathway for the reaction $CCl_2F_2 + F_{surf} \rightarrow CClF_3 + Cl_{surf}$ (eqn (2)) on the defect free β-AlF$_3$ (100) (1 × 1) surface. The reaction coordinate is the cumulative minimised distance between images along the pathway.
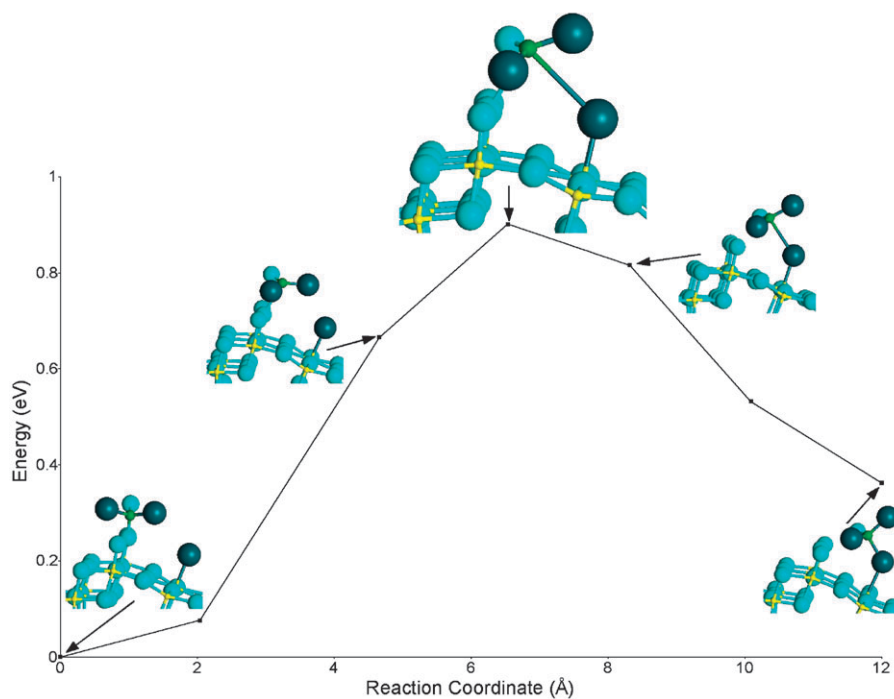
Fig. 7 The lowest energy pathway for the reaction $CCl_2F_2 + Cl_{surf} \rightarrow CCl_3F + F_{surf}$ (eqn (3)) on the defect free β-AlF$_3$ (100) (1 × 1) surface. The reaction coordinate is the cumulative minimised distance between images along the pathway.

where m_i is the mass of the gas molecule, h is the Planck constant and p_i is the partial pressure of the gas. The chemical potential of a gas such as CCl_2F_2 also contains terms due to

the internal degrees of freedom of the molecule. It can be assumed that these terms will be dominated by the vibrational degrees of freedom, which will only change by a small amount

This journal is © the Owner Societies 2010

Phys. Chem. Chem. Phys., 2010, **12**, 6124–6134 | 6131

after adsorption. To a good approximation, therefore, the errors associated with setting the chemical potential of CCl_2F_2 to that of an ideal gas and q_{vib} in eqn (8) to unity will cancel, hence

$$\mu_{CCl_2F_2} = kT\left[\ln\frac{\theta}{1-\theta} + \frac{E_{ads}}{kT}\right], \qquad (10)$$

and therefore,

$$\frac{\theta}{1-\theta} = \exp\left(\frac{\mu_{CCl_2F_2} - E_{ads}}{kT}\right). \qquad (11)$$

The binding energy of CCl_2F_2, at low coverages, to the defect free surface is around -0.15 eV for adsorption *via* a Cl atom (see section III.C). Using eqn (9), $\mu = -1.01$ eV at 600 K for CCl_2F_2 at standard pressure. It is, therefore, estimated that at 600 K approximately one in every 3×10^7 of the under-coordinated Al ions will be covered by a CCl_2F_2 molecule adsorbed *via* its Cl ion. Approximately 83% of the under-coordinated Al ions on this surface will be in a defect free region (1 in 6 [17%] of the monodentate F ions are involved in defects consisting of two adjacent monodentate F ions (Table 1)). Assuming a reaction barrier, $\Delta E^\ddagger$, of 1.48 eV and a value of one for the ratio between the transition and initial state vibrational partition functions, the reaction rate constant is 5 s^{-1}. The overall turnover is $(0.83 \times 5)/(3 \times 10^7) = 1 \times 10^{-7}$ s^{-1} per Al site. The rate constant and associated data for this reaction pathway are summarised in Table 8. Data for analogous reaction pathways at both defect sites (two and three adjacent under-coordinated Al ions) are also displayed as are data for the reaction pathway of step two of the reaction at a defect free surface. Step one of the reaction is predicted to occur predominately at defect sites on the surface of β-AlF$_3$ (100).

When the surface and the reactants are in dynamic equilibrium the number of Cl ions on the surface remains constant, hence, the turnover rates of step one and step two of the reaction will be equal. The rate constant for the second step of the reaction is significantly greater than that of the first step, hence, the number of Cl ions present on the surface will be very small (as the turnover rate of step two is proportional to the amount of Cl present). The overall rate for the reaction, to a very good approximation, will be determined by the rate of step one of the reaction. Step one of the dismutation reaction is, therefore, the rate limiting step. It is possible that the turnover of the second step could be even greater at defect sites, but as this step is not rate limiting we have not investigated such possibilities.

Experimental data suggests[46] that the turnover rate per Al site is much higher than that predicted from our calculations. In a recent experiment,[46] a micro-reactor was used to investigate the dismutation of CCl_2F_2 over a β-AlF$_3$ catalyst. The micro-reactor was filled with around 20 mg of the β-AlF$_3$ material and a gas consisting of a 3:1 ratio of He to CCl_2F_2 was passed through the micro-reactor at a rate of 100 cm^3 min^{-1}. The residence time of the gas through the reactor was around one second, during which time approximately 33% of the reactant underwent a dismutation reaction at 663 K. This corresponds to 1×10^{18} CCl_2F_2 molecules undergoing the dismutation reaction per second. If it is assumed that the β-AlF$_3$ catalyst has a surface area of approximately 20 m^{2}g^{-1} with two under-coordinated Al ions per nm^2 and that 4% of these Al ions are reactive, then we estimate that there are approximately 3×10^{16} active Al sites in the reactor. The turnover rate is, therefore, on the order of one hundred CCl_2F_2 molecules per second per Al site. There are, however, many assumptions made in this calculation. Perhaps the largest unknown is the number of catalytic sites on the β-AlF$_3$ surface. It is assumed that active sites are only exposed on the (100) surface and that this surface makes up 4% of the total surface area exposed.[27] The figure of 4% is obtained from a Wulff plot based on the energies of the (100), (010) and (001) surfaces and assumes the crystallites are in thermodynamic equilibrium. If the crystallites are not in thermodynamic equilibrium, then the amount of the (100) surface that is exposed could perhaps differ by an order of magnitude in either direction. It is, however, possible for the (100) surface to micro-facet, reducing the overall number of sites, possibly by an order of magnitude. Given these assumptions the number of sites may be under-estimated by a factor of 10 or over-estimated by up to a factor of 100. This leads to an estimate of the turnover of between 10 and 10000 CCl_2F_2 molecules per second per Al site. The experimental turnover is significantly greater than the turnover of 6×10^{-5} s^{-1} per Al site predicted from our calculations. The turnover is predicted at 600 K in our calculation whereas experimentally the reaction was shown to proceed at 663 K. At 663 K the calculated turnover is 2×10^{-3} s^{-1}, which is still very low.

Calculating reaction rates from transition state theory is well known to be a very difficult problem,[47] especially for large complex systems such as the one studied in this paper. Accurate determination of the potential energy surface is required. There may be many accessible pathways that contribute significantly to the overall rate constant. There are, also, a number of failings of transition state theory. The effects of quantum tunnelling are not included, although for

Table 8 The turnover rates and associated data for several reaction pathways at 600 K. The fractions of sites available are calculated from data in Table 1 and the values for the CCl_2F_2 binding energies are discussed in section III.C. The turnover for step two is calculated assuming that there is always a surface Cl ion available for the reaction

Description of pathway	Fraction of Sites	CCl_2F_2 binding energy (eV)	Fraction of sites covered	Energy barrier, $\Delta E^\ddagger$ (eV)	Rate constant (s^{-1})	Turnover (molecules s^{-1} per Al site)
Step 1 (defect free)	0.83	-0.15	3×10^{-8}	1.48	5×10^0	1×10^{-7}
$\begin{bmatrix}\circ\bullet\bullet\circ\\\bullet\circ\circ\circ\end{bmatrix}$	0.17	-0.25	2×10^{-7}	1.20	1×10^3	4×10^{-5}
$\begin{bmatrix}\circ\bullet\bullet\bullet\circ\\\bullet\circ\circ\circ\bullet\end{bmatrix}$	0.0006	-0.35	1×10^{-6}	1.04	2×10^4	2×10^{-5}
Step 2 (defect free)	1.0	-0.20	8×10^{-8}	0.89	4×10^5	3×10^{-2}

high barriers this effect is very small. It does not include the effects of dynamical recrossings of the transition state, that is, it assumes that every barrier crossing event proceeds directly to the products, and hence the rate constant may be over-estimated.[48–50]

In our work, there is a very large discrepancy between the experimental turnover and the turnover predicted from our proposed reaction pathway. These errors may be due to inaccurate representations of the potential energy surface and the failings of transition state theory. It has been shown in this paper, however, that relatively subtle differences in the local geometry of the AlF$_3$ surface can dramatically influence the energy barrier of a given reaction. For instance the transition state energy for the indirect diffusion of F ions was around 1.3 eV for three of the four pathways considered but 1.0 eV for the other pathway (section III.B). Defect sites could contribute to, or even dominate, the overall reaction rate. For example, a fluorine vacancy in the first few layers of the surface could have a dramatic effect on the reactivity of a local catalytic Al site. It is, therefore, possible that the reaction could proceed *via* the reaction mechanism that we have proposed but at a defective site that we have not considered. The sensitivity of reaction rates to small changes in geometry could also explain why HS-AlF$_3$ shows significantly greater catalytic activity than β-AlF$_3$. HS-AlF$_3$ is thought to contain a significant number of Al ions in distorted environments; some of these sites may significantly reduce the energy barrier of a given reaction mechanism.

IV. Conclusions

In this paper the distribution of monodentate F ions on the β-AlF$_3$ (100) surface was calculated. The diffusion of these F ions across the surface was then considered. Adsorption of CCl$_2$F$_2$ to the β-AlF$_3$ surface was investigated and possible reaction pathways for the dismutation of 2CCl$_2$F$_2$ $\rightarrow$ CClF$_3$ + CCl$_3$F were calculated.

It was predicted that the majority of the monodentate F ions on the surface of β-AlF$_3$ (100) are evenly distributed. At 600 K, however, 17% of the F ions on the surface are predicted to be adjacent to another such F ion and around 0.06% will be adjacent to two such F ions. Over 99% of these groupings of F ions will be on row A of the surface. Two competing mechanisms for the diffusion of F ions across the surface of β-AlF$_3$ were considered. It was shown that these mechanisms both have similar energetics and that the local environment determines which one provides the lowest energy barrier. Consequently, both types of mechanism are predicted to occur. It was demonstrated that, under typical reaction temperatures (600 K), the surface F ions are mobile, moving between Al ions on a timescale of several hops per ms. The surface will, therefore, be in thermodynamic equilibrium on the experimental timescale.

A reaction mechanism for the dismutation of CCl$_2$F$_2$ to form CCl$_3$F and CClF$_3$ on the surface of β-AlF$_3$ (100) was proposed. This mechanism involves the participation of surface F ions and occurs *via* a two step process. Analysis of the reaction barriers suggests that this reaction could plausibly occur on the β-AlF$_3$ (100) surface at elevated temperatures,

although not with the rate constants observed experimentally. The processes that contribute most significantly to the overall turnover are the reactions corresponding to eqn (2) occurring at defect sites. This demonstrates the extent to which a small change to the local structure of the surface can dramatically increase the rate of a reaction. Due to the huge number of possible defects that could occur at a surface, it is prohibitively expensive computationally to consider all such possibilities. The sensitivity of the reaction barrier to local geometric structure may, however, explain why HS-AlF$_3$ is highly reactive. It may be that only a relatively small number of defect sites are responsible for its high catalytic activity.

References

1 S. K. Rüdiger, U. Groß, M. Fiest, H. A. Prescott, S. C. Shekar, S. I. Troyanov and E. Kemnitz, *J. Mater. Chem.*, 2005, **15**, 588.
2 E. Kemnitz, U. Groß S. Rüdiger and S. C. Shekar, *Angew. Chem.*, 2003, **115**, 4383.
3 E. Kemnitz and D. H. Menz, *Prog. Solid State Chem.*, 1998, **26**, 97.
4 L. E. Manzer and V. N. M. Rao, *U.S. Patent*, 4,902,838, 1990.
5 L. E. Manzer and V. N. M. Rao, *Adv. Catal.*, 1993, **39**, 329.
6 D. R. Corbin and V. N. M. Rao, *U.S. Patent*, 2000, 6,040,486.
7 R. Hoppe and D. Kissel, *J. Fluorine Chem.*, 1984, **24**, 327.
8 P. Daniel, A. Bulou, M. Rousseau, J. Nouet, J. L. Fourquet, M. Leblanc and R. Burriel, *J. Phys.: Condens. Matter*, 1990, **2**, 5663.
9 A. Le Bail, C. Jacoboni, M. Leblan, R. De Pape, H. Duroy and J. F. Fourquet, *J. Solid State Chem.*, 1988, **77**, 96.
10 E. Kemnitz and J. M. Winfield, *Advanced Inorganic Fluorides: Synthesis, Characterization and Applications*, Elsevier Science, New York, 2000.
11 E. DeCanio, J. W. Bruno, V. P. Nero and J. C. Edwards, *J. Catal.*, 1993, **140**, 84.
12 P. J. Chupas, M. F. Ciraolo, J. C. Hanson and C. P. Grey, *J. Am. Chem. Soc.*, 2001, **123**, 1694.
13 L. Fischer, V. Harl, S. Kastelan and J. B. d'Espinose de la Caillerie, *Solid State Nucl. Magn. Reson.*, 2000, **16**, 85.
14 G. B. McVicker, C. J. Kim and J. J. Eggert, *J. Catal.*, 1983, **80**, 315.
15 M. Saniger, N. A. Sanchez and J. O. Flores, *J. Fluorine Chem.*, 1998, **88**, 117.
16 T. J. Skapin, *J. Mater. Chem.*, 1995, **5**, 1215.
17 A. Vimont, J. C. Lavalley, L. Francke, A. Demourgues, A. Tressaud and M. Daturi, *J. Phys. Chem. B*, 2004, **108**, 3246.
18 A. Demourgues, L. Francke, E. Durant and A. Tressaud, *J. Fluorine Chem.*, 2002, **114**, 229.
19 A. Hess and E. Kemnitz, *J. Catal.*, 1994, **149**, 449.
20 A. Hess, E. Kemnitz, A. Lippitz, W. E. S. Unger and D. H. Menz, *J. Catal.*, 1994, **148**, 270.
21 S. S. Deshmukh, V. I. Kovalchuk, V. Y. Borovkov and J. L. Deitri, *J. Phys. Chem. B*, 2000, **104**, 1277.
22 A. Wander, C. L. Bailey, S. Mukhopadhyay, B. G. Searle and N. M. Harrison, *J. Mater. Chem.*, 2006, **16**, 1906.
23 C. L. Bailey, S. Mukhopadhyay, A. Wander, B. G. Searle and N. M. Harrison, *J. Phys. Chem. C*, 2009, **113**, 4976.
24 C. L. Bailey, A. Wander, S. Mukhopadhyay, B. G. Searle and N. M. Harrison, *J. Chem. Phys.*, 2008, **128**, 224703.

This journal is © the Owner Societies 2010

Phys. Chem. Chem. Phys., 2010, **12**, 6124–6134 | 6133

25 K. Sohlberg, S. T. Pantelides and S. J. Pennycook, *J. Am. Chem. Soc.*, 2001, **123**, 26.

26 C. L. Bailey, S. Mukhopadhyay, A. Wander and N. M. Harrison, *Journal of Physics: Conference Proceedings*, 2008, **100**, 012009.

27 A. Wander, C. L. Bailey, S. Mukhopadhyay, B. G. Searle and N. M. Harrison, *J. Phys. Chem. C*, 2008, **112**, 6515.

28 E. Kemnitz and D. Menz, *Z. Anorg. Allg. Chem.*, 1990, **589**, 228.

29 L. Rowley, G. Webb, J. M. Winfield and A. McCulloch, *Appl. Catal.*, 1989, **52**, 69.

30 G. Kijowski, G. Webb and J. M Winfield, *J. Fluorine Chem.*, 1985, **27**, 213.

31 A. Hess and E. Kemnitz, *Appl. Catal., A*, 1992, **82**, 247.

32 A. Hammoudeh, S. S. Mahmoud and S. Gharaibeh, *Appl. Catal., A*, 2003, **243**, 147.

33 K. Laidler and C. King, *J. Phys. Chem.*, 1983, **87**, 2657.

34 R. Dovesi, V. R. Saunders, C. Roetti, R. Orlando, C. M. Zicovich-Wilson, F. Pascale, B. Civalleri, K. Doll, N. M. Harrison, I. J. Bush, P. D'Arco and M. Llunell, *CRYSTAL 2006 User's Manual*, University of Torino, 2007.

35 A. D. Becke, *J. Chem. Phys.*, 1993, **98**, 1372.

36 S. H. Vosko, L. Wilk and M. Nusair, *Can. J. Phys.*, 1980, **58**, 1200.

37 P. J. Stephens, F. J. Devlin, C. F. Chabalowski and M. J. Frisch, *J. Phys. Chem.*, 1994, **98**, 11623.

38 J. Muscat, A. Wander and N. M. Harrison, *Chem. Phys. Lett.*, 2001, **342**, 397.

39 A. Wander, C. L. Bailey, B. G. Searle, S. Mukhopadhyay and N. M. Harrison, *Phys. Chem. Chem. Phys.*, 2005, **7**, 3989.

40 G. Henkelman and H. Jónsson, *J. Chem. Phys.*, 2000, **113**, 9978.

41 G. Henkelman, B. P. Uberuaga and H. Jónsson, *J. Chem. Phys.*, 2000, **113**, 9901.

42 C. L. Bailey, A. Wander, B. G. Searle and N. M. Harrison, *DL Technical Report*, DL-TR-2005-003, 2005, Avail. from http://epubs.cclrc.ac.uk/work-details?w = 40462.

43 S. F. Boys and F. Bernardi, *Mol. Phys.*, 1970, **19**, 553.

44 C. L. Bailey, A. Wander, S. Mukhopadhyay, B. G. Searle and N. M. Harrison, *Phys. Chem. Chem. Phys.*, 2008, **10**, 2918.

45 J. B. Hudson, *Surface Science: An Introduction*, John Wiley and Sons, Inc., 1998.

46 E. K. L. Y. Hajime, J. L. Delattre and A. M. Stacy, *Chem. Mater.*, 2007, **19**, 894.

47 D. G. Truhlar, B. C. Garrett and S. J. Klippenstein, *J. Phys. Chem.*, 1996, **100**, 12771.

48 C. H. Bennett, in *Algorithms for Chemical Computations*, ed. R. E. Christofferson, American Chemical Society, Washington, DC, 1977, pp. 63–97.

49 D. Chandler, *J. Chem. Phys.*, 1978, **68**, 2959.

50 J. B. Anderson, *J. Chem. Phys.*, 1973, **58**, 4684.